NMR Evidence for Universal Pseudogap Behavior in Quasi-Two-Dimensional FeSe-Based Superconductors

B. L. Kang(康宝蕾)[1†], M. Z. Shi(石孟竹)[1†], D. Zhao(赵丹)[1], S. J. Li(李顺姣)[1], J. Li(李建)[1], L. X. Zheng(郑立玄)[1], D. W. Song(宋殿武)[1], L. P. Nie(聂林鹏)[1], T. Wu(吴涛)[1,2,3,4,5*], and X. H. Chen(陈仙辉)[1,2,3,4,5*]

[1]*Hefei National Research Center for Physical Sciences at the Microscale, University of Science and Technology of China, Hefei 230026, China*
[2]*Key Laboratory of Strongly coupled Quantum Matter Physics, Department of Physics, University of Science and Technology of China, Hefei 230026, China*
[3]*CAS Center for Excellence in Superconducting Electronics (CENSE), Shanghai 200050, China*
[4]*Collaborative Innovation Center of Advanced Microstructures, Nanjing University, Nanjing 210093, China*
[5]*Hefei National Laboratory, University of Science and Technology of China, Hefei 230088, China*

(Received 20 September 2022; accepted manuscript online 31 October 2022)

Recently, by intercalating organic ions into bulk FeSe superconductors, two kinds of layered FeSe-based superconductors [$(TBA)_xFeSe$ and $(CTA)_xFeSe$] with superconducting transition temperatures (T_c) above 40 K have been discovered. Due to the large interlayer distance (∼15 Å), these new layered superconductors have a large resistivity anisotropy analogous to bismuth-based cuprate superconductors. Moreover, remarkable pseudogap behavior well above T_c is revealed by nuclear magnetic resonance (NMR) measurements on ^{77}Se nuclei, suggesting a preformed pairing scenario similar to that of cuprates. Here, we report another new kind of organic-ion-intercalated FeSe superconductor, $(PY)_xFeSe$, with a reduced interlayer distance (∼10 Å) compared to $(TBA)_xFeSe$ and $(CTA)_xFeSe$. By performing ^{77}Se NMR and transport measurements, we observe a similar pseudogap behavior well above T_c of ∼40 K and a large resistivity anisotropy of $\sim 10^4$ in $(PY)_xFeSe$. All these facts strongly support a universal pseudogap behavior in these layered FeSe-based superconductors with quasi-two-dimensional electronic structures.

DOI: 10.1088/0256-307X/39/12/127401

Cooper pairing and superconducting phase coherence are two indispensable prerequisites for realizing macroscopic superconductivity, which occurs simultaneously in Bardeen–Cooper–Schrieffer (BCS) superconductors. In contrast, Cooper pairing occurs prior to superconducting phase coherence in high-T_c cuprate superconductors, which has been used to account for the well-known pseudogap phenomenon.[1–3] In this sense, superconducting transition temperature (T_c) is determined by phase coherence instead of Cooper pairing.[1] Although whether the preformed Cooper pairing can persist up to the pseudogap temperature is still under debate, evidence for fluctuating superconductivity is widely observed to be well above T_c in cuprates.[2,4–6] Recently, the evidence for fluctuating superconductivity above T_c was also reported in heavily hole-doped cuprates $Bi_2Sr_2CaCu_2O_{8+\delta}$ (Bi2212), which further strengthens the above picture and suggests a generic nature of superconductivity in cuprates.[7] How to understand the preformed Cooper pairing well above T_c is still an open question.

In iron-based superconductors, whether preformed Cooper pairing exists remains elusive experimentally.[8–13] The discovery of high-T_c superconductivity in a single-layer $FeSe/SrTiO_3$ film (FeSe/STO) sheds new light on this issue.[14] Although FeSe/STO exhibits a large superconducting gap of approximately 20 meV with a gap opening temperature of approximately 65 K, the zero-resistance temperature determined by transport measurement is always lower than 40 K.[15–18] These results strongly suggest a possible pseudogap behavior due to preformed Cooper pairing in FeSe/STO films. Recently, two kinds of organic-ion-intercalated FeSe-based superconductors have been successfully synthesized with T_c above 40 K, which exhibit a quasi-two-dimensional (quasi-2D) electronic structure analogous to bismuth-based cuprate superconductors.[19–21] Interestingly, a pseudogap behavior similar to that in cuprates has been revealed to be well above T_c by nuclear magnetic resonance (NMR) measurements, suggesting the existence of preformed Cooper pairing.[19] Meanwhile, the preformed Cooper pairing picture is further supported by angle-resolved photoemission spectroscopy (ARPES) and *in situ* transport measurements on single-layer FeSe/STO.[22,23] On the other hand, it is quite confusing that pseudogap behavior has not been reported in layered FeAs-based superconductors or other layered FeSe-based superconductors, including $CsCa_2Fe_4As_4F_2$[24] and (Li,Fe)OHFeSe.[25] To date, how to understand the origin of pseudogap behavior in organic-ion-intercalated FeSe-based superconductors and FeSe/STO films is still under debate. Whether the quasi-

†These authors contributed equally to this work.
*Corresponding authors. Email: wutao@ustc.edu.cn; chenxh@ustc.edu.cn
© 2022 Chinese Physical Society and IOP Publishing Ltd

2D electronic structure is a necessary condition for observing pseudogap behavior also needs more investigation.

In this work, a new kind of organic-ion-intercalated FeSe superconductor $(PY)_xFeSe$ ($x \sim 0.15$) was successfully synthesized with $T_c \sim 40\,K$ (see the Supplemental Material). Through the intercalation of organic ions 1-butyl-1-methylpyrrolidinium (PY^+), the distance between adjacent FeSe layers is expanded to 10.5 Å, which is smaller than the ∼15 Å of $(CTA)_xFeSe$ and $(TBA)_xFeSe$ but close to the 9.32 Å of (Li,Fe)OHFeSe. As is commonly believed, charge transfer from organic ions to FeSe layers plays an essential role in achieving a high-T_c superconductivity of approximately 40 K.[15,18,26,27] On the other hand, the enlarged interlayer distance would also weaken the interlayer coupling compared to bulk FeSe. As shown in Fig. 1, through the intercalation of various organic ions from (PY^+) to (TBA^+), the distance between adjacent FeSe layers is largely expanded with a similar layered structure. By measuring the Knight shift and nuclear spin-lattice relaxation rate, a pseudogap behavior similar to that in $(CTA)_xFeSe$ and $(TBA)_xFeSe$ is revealed below $T_p \sim 60\,K$ in $(PY)_xFeSe$. Moreover, the electrical transport measurement also reveals a large resistivity anisotropy up to $\sim 10^4$, supporting a quasi-2D electronic structure. These results indicate that the pseudogap behavior in these new layered FeSe-based superconductors is tied to a quasi-2D electronic structure instead of the interlayer distance, which may explain the absence of pseudogap behavior in other layered iron-based superconductors with moderate resistivity anisotropy [e.g., (Li,Fe)OHFeSe].

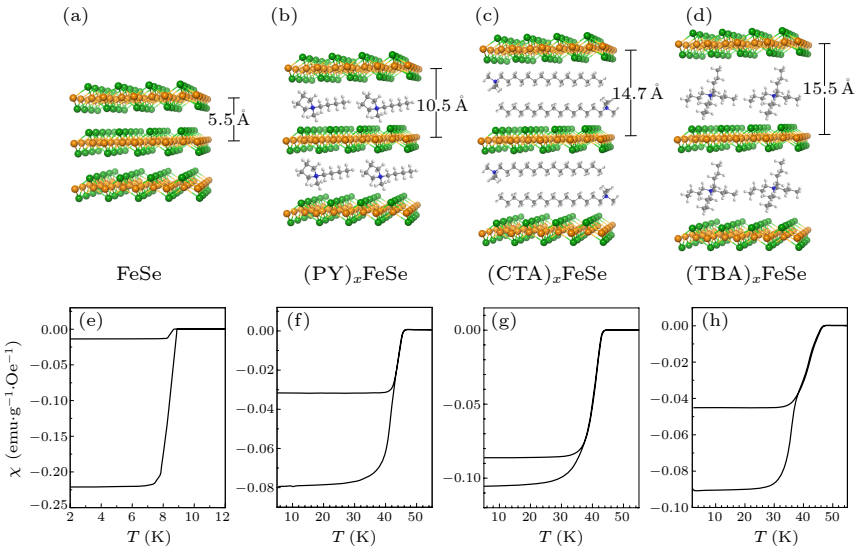

Fig. 1. Crystal structures of (a) FeSe, (b) $(PY)_xFeSe$, (c) $(CTA)_xFeSe$, and (d) $(TBA)_xFeSe$. Accurate molecular selection enables fine tuning of the interlayer distance d. Temperature dependence of the magnetic susceptibility measured in field-cooling (FC) and zero-field-cooling (ZFC) modes under a magnetic field of 5 Oe applied out of plane for (e) FeSe, (f) $(PY)_xFeSe$, (g) $(CTA)_xFeSe$, and (h) $(TBA)_xFeSe$.

It is well known that NMR is a bulk-sensitive technique to probe pseudogap behavior since it provides a direct measure of local spin susceptibility (χ_s).[28,29] In cuprate superconductors, the pseudogap manifests as a simultaneous reduction in the Knight shift (K) and nuclear spin-lattice relaxation rate ($1/T_1$).[30,31] Usually, the total Knight shift can be divided into two parts with $K_{tot} = K_s + K_{orb}$, where K_{orb} is a temperature-independent orbital shift and K_s is a temperature-dependent spin shift. The spin shift is related to the uniform spin susceptibility with $K_s = A\chi_s$, where A is the hyperfine coupling tensor between nuclear and electronic spins. The nuclear spin-lattice relaxation rate is related to dynamical spin susceptibility and can be expressed as $1/T_1T \sim \sum_q \gamma_n^2 |A_\perp(q)|^2 \chi''(q,\omega)/\omega$, where $A_\perp(q)$ is the transverse hyperfine form factor and $\chi''(q,\omega)$ is the imaginary part of the dynamical susceptibility in the direction perpendicular to the external field. In a conventional Fermi-liquid picture, $1/T_1T$ and K_s follow a simple Korringa relation with $1/T_1T \sim K_s^2 \sim N(E_F)^2$, where $N(E_F)$ is the density of states at Fermi energy. In this context, both K_s and $1/T_1T$ can be used to measure the suppression of $N(E_F)$ due to the formation of a pseudogap.

In Fig. 2, the ^{77}Se NMR evidence for pseudogap behavior in three organic-ion-intercalated FeSe-based superconductors is summarized, including the new result of $(PY)_xFeSe$ and the previously reported results of $(CTA)_xFeSe$ and $(TBA)_xFeSe$.[19] To improve the signal-to-noise ratio, 50% ^{77}Se isotope-enriched samples were used in the measurement of $(PY)_xFeSe$ and $(TBA)_xFeSe$. As shown in Figs. 2(a)–2(c), the temperature-dependent Knight shift of ^{77}Se nuclei shows a clear deviation from its high-temperature behavior below 60 K, which was ascribed to preformed Cooper pairing in previous work.[19] The absence of any change in the NMR spectral profile indicates that the shift of the NMR spectrum to a low frequency below 60 K comes from an intrinsic suppression of the uniform spin susceptibility (also see the Supplemental Material).[19] As shown in Figs. 2(d)–2(f), a similar deviation from the high-temperature behavior is also observed in the temperature-dependent $1/T_1T$ below ∼60 K. The similar temperature-dependent behavior in both the Knight shift and $1/T_1T$ confirms that the observed pseudo-

gap behavior should originate from quasiparticle-like excitations. More analysis of the temperature-dependent evolution of the Korringa ratio over the whole temperature range will be discussed elsewhere. In summary, the above NMR results display a universal pseudogap behavior in these organic-ion-intercalated FeSe-based superconductors with the characteristic temperature $T_{\rm p} \sim 60\,{\rm K}$. In addition, the observed pseudogap behavior in NMR measurements is almost independent of field orientation or strength in our present field range (see the Supplemental Material), which is consistent with the large pairing gap (∼16 meV) observed by scanning tunneling microscopy/spectroscopy (STM/S) experiments.[19]

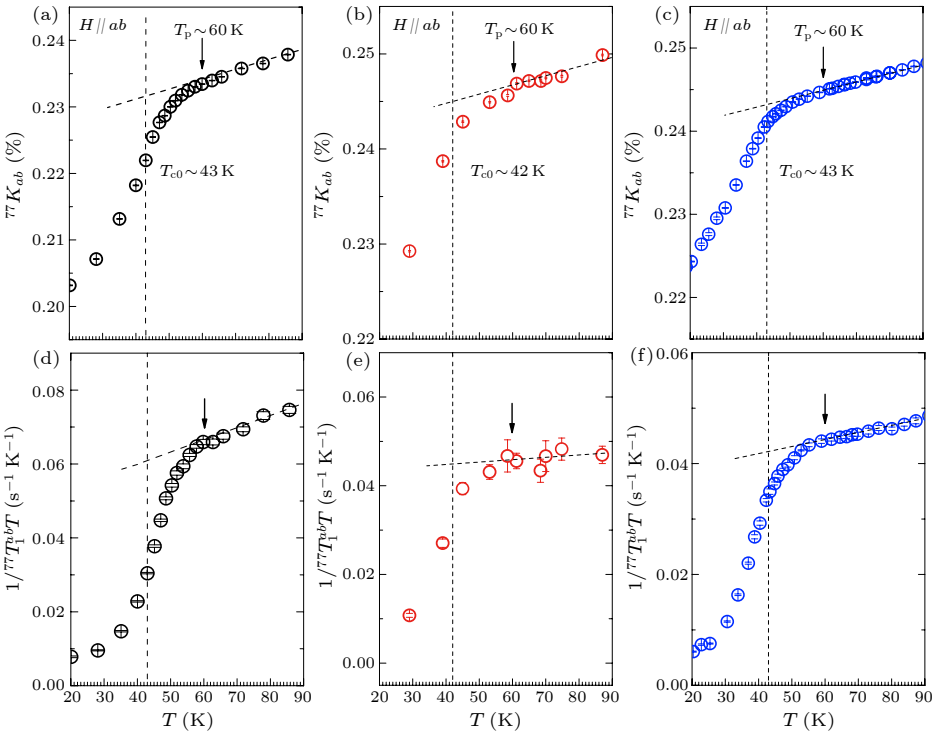

Fig. 2. (a)–(c) Temperature dependence of the Knight shift $^{77}K_{ab}$ for $(PY)_x$FeSe, $(CTA)_x$FeSe, and $(TBA)_x$FeSe with an external magnetic field applied along ab plane. (d)–(f) Temperature evolution of the spin-lattice relaxation rate divided by temperature, $1/^{77}T_1^{ab}T$, for $(PY)_x$FeSe, $(CTA)_x$FeSe, and $(TBA)_x$FeSe with an external magnetic field applied along ab plane. The external magnetic field is ∼12 T. The data of $(CTA)_x$FeSe and $(TBA)_x$FeSe are taken from Ref. [19].

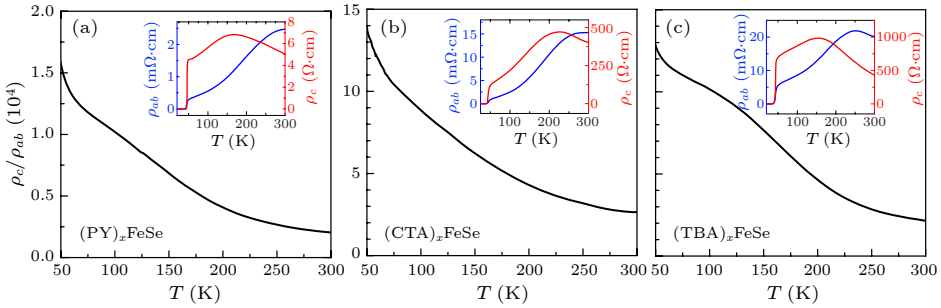

Fig. 3. The anisotropy ratio of electrical transport ρ_c/ρ_{ab} for (a) $(PY)_x$FeSe, (b) $(CTA)_x$FeSe, and (c) $(TBA)_x$FeSe. The inset shows the temperature dependence of in-plane and out-of-plane resistivity in the temperature range of 20–300 K. The results indicate an extremely large anisotropy ratio of up to 10^4 in these intercalated FeSe-based superconductors, which suggests a quasi-2D electronic structure. The data of $(CTA)_x$FeSe and $(TBA)_x$FeSe are taken from Ref. [19].

To verify the dimensionality of the electronic structure, the in-plane and out-of-plane resistivities (ρ_{ab} and ρ_c) were also measured in these organic-ion-intercalated FeSe-based superconductors. As shown in Fig. 3, it is clear that all the three samples exhibit a similar temperature-dependent resistivity anisotropy (ρ_c/ρ_{ab}). Although the anisotropy ratio of $(PY)_x$FeSe reaches $\sim 10^4$ at 50 K, this value is one order of magnitude smaller than $\sim 10^5$ for $(CTA)_x$FeSe and $(TBA)_x$FeSe.[19] Considering the smaller interlayer distance in $(PY)_x$FeSe, this result is quite reasonable. As shown in the inset of Fig. 3, while the in-plane resistivity ρ_{ab} displays metallic behavior over almost

the whole temperature range, the out-of-plane resistivity ρ_c of the three samples exhibits a similar hump behavior from 150 K to 200 K, suggesting a possible electronic crossover.[32] It should be noted that, regardless of the interlayer distance, the large value of the anisotropy ratio above $\sim 10^4$ strongly supports a generic quasi-2D electronic structure in these organic-ion-intercalated FeSe-based superconductors, which exhibit a great similarity to bismuth-based cuprate superconductors.[20,21] We think that this should be an important prerequisite for the emergence of pseudogap behavior in these samples. Next, we will discuss the correlation between the anisotropy ratio and pseudogap behavior by involving more iron-based superconductors.

As shown in Fig. 4, the relationship between ρ_c/ρ_{ab} and interlayer distance d is summarized for several selected layered iron-based superconductors and cuprates. Empirically, the anisotropy ratio, which reflects the 2D nature of the electronic structure, should be enhanced by increasing the interlayer distance. However, in practice, it usually depends on what kind of blocking layer is used in the layered structure. For example, with a comparable interlayer distance of $\sim$10 Å, the anisotropy ratio of $Ca_{10}(Pt_4As_8)((Fe_{0.86}Pt_{0.14})_2As_2)_5$ with metallic blocking layers is much smaller than that of (Li,Fe)OHFeSe and $(PY)_x$FeSe with insulating blocking layers. Therefore, the 2D nature of the electronic structure also depends on the nature of the blocking layers.

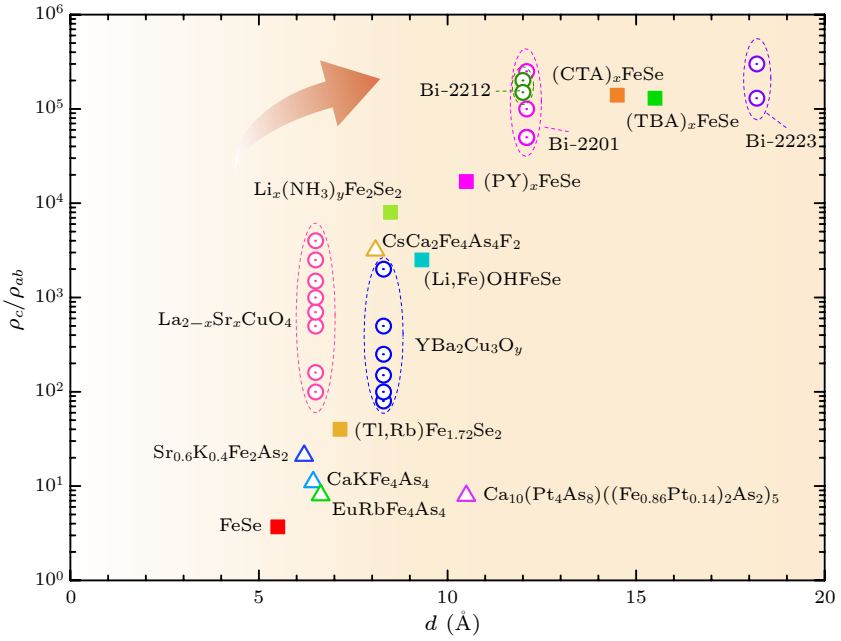

Fig. 4. A summarized ρ_c/ρ_{ab} plot for a series of layered high-T_c superconductors. The data points labeled in filled squares, open triangles, and open circles represent FeSe-based superconductors, FeAs-based superconductors, and cuprates, respectively. The d of cuprates is defined as the Cu–O single-layer, double-layer or tri-layer separations. The data points except for $(PY)_x$FeSe are taken from Refs. [19,32–56].

Our new results indicate that the newly discovered organic-ion-intercalated FeSe-based superconductors [$(PY)_x$FeSe, $(CTA)_x$FeSe, and $(TBA)_x$FeSe] display a generic quasi-2D electronic structure with an anisotropy ratio above $\sim 10^4$, in which universal pseudogap behavior is observed. In contrast, pseudogap behavior is absent in (Li,Fe)OHFeSe with an anisotropy ratio of only approximately 10^3. Furthermore, most FeAs-based superconductors also exhibit a smaller anisotropy ratio than organic-ion-intercalated FeSe-based superconductors. As shown in Fig. 4, the anisotropy ratio of $CsCa_2Fe_4As_4F_2$, which has the largest anisotropy ratio among all FeAs-based superconductors, is only $\sim 10^3$. Accordingly, there has been no evidence for the existence of pseudogap behavior in FeAs-based superconductors. These facts suggest that the extremely 2D electronic structure should play a crucial role in the emergence of pseudogap behavior in these organic-ion-intercalated FeSe-based superconductors. In addition, the nearly same pairing temperature of $\sim$60 K in these organic-ion-intercalated FeSe-based superconductors is ascribed to the similar electron doping level and quasi-2D electronic structure in these materials. This could also be used to explain the possible pseudogap behavior in the FeSe/STO film due to a 2D electronic structure.[14–18] Recent ARPES and *in situ* transport measurements further support the preformed Cooper pairing picture in the FeSe/STO film.[22,23] On the other hand, a similar pseudogap behavior due to preformed Cooper pairing has also been revisited in overdoped Bi2212.[7] The quantitative theoretical calculation indicates that a von Hove singularity close to the Fermi level may further boost the 2D superconducting fluctuations. Whether superconducting fluctuations due to phase fluctuations are enough to account for the pseudogap behavior up to 60 K still needs more theoretical investigations in these organic-ion-intercalated FeSe-based superconductors. On the other hand, the physics of BCS-BEC crossover has also been discussed in iron chalcogenide superconductors recently,[8,57–60] which

may be one possible picture to account for the above-mentioned preformed Cooper pairing. In the BCS-BEC crossover regime, the coherence length of Cooper pair (ξ) is required to be comparable to $1/k_{\rm F}$, where $k_{\rm F}$ is the Fermi wave vector. Equivalently, the ratio of the pairing gap Δ to the bandwidth or Fermi energy $E_{\rm F}$ is also required to be of order unity ($\Delta/E_{\rm F} \sim 1$). Except for bulk FeSe, in most heavily electron-doped FeSe-based superconductors including $K_{0.8}Fe_2Se_2$ and (Li,Fe)OHFeSe, the $\Delta/E_{\rm F}$ is closer to the BCS limit rather than the BCS-BEC crossover regime.[59,61] In our case, since the organic-ion-intercalated FeSe-based superconductors own a comparable pairing gap and similar electron doping level with (Li,Fe)OHFeSe, the BCS-BEC crossover is also less possible for the emergence of preformed Cooper pairing.

In summary, our present work reveals a universal pseudogap behavior tied to quasi-2D electronic structures in newly discovered organic-ion-intercalated FeSe-based superconductors. These results also offer a natural explanation for the mysterious superconducting behavior in the FeSe/STO film, suggesting a generic nature of 2D superconductivity in this system. Finally, the similar pseudogap behavior observed in both bismuth-based cuprates and layered FeSe-based superconductors with quasi-2D electronic structures should be key to understanding the nature of high-$T_{\rm c}$ superconductivity.

Acknowledgments. This work was supported by the National Natural Science Foundation of China (Grant Nos. 11888101 and 12034004), the National Key R&D Program of China (Grant No. 2017YFA0303000), the Strategic Priority Research Program of Chinese Academy of Sciences (Grant No. XDB25000000), the Anhui Initiative in Quantum Information Technologies (Grant No. AHY160000), and the Innovation Program for Quantum Science and Technology (Grant No. 2021ZD0302800).

References

[1] Emery V J and Kivelson S A 1995 *Nature* **374** 434
[2] Corson J, Mallozzi R, Orenstein J, Eckstein J N, and Bozovic I 1999 *Nature* **398** 221
[3] Uemura Y J *et al.* 1989 *Phys. Rev. Lett.* **62** 2317
[4] Wang Y Y, Li L, and Ong N P 2006 *Phys. Rev. B* **73** 024510
[5] Tallon J L, Storey J G, and Loram J W 2011 *Phys. Rev. B* **83** 092502
[6] Li L, Wang Y Y, Komiya S, Ono S, Ando Y, Gu G D, and Ong N P 2010 *Phys. Rev. B* **81** 054510
[7] He Y, Chen S D, Li Z X, Zhao D, Song D, Yoshida Y, Eisaki H, Wu T, Chen X H, Lu D H, Meingast C, Devereaux T P, Birgeneau R J, Hashimoto M, Lee D H, and Shen Z X 2021 *Phys. Rev. X* **11** 031068
[8] Kasahara S, Yamashita T, Shi A, Kobayashi R, Shimoyama Y, Watashige T, Ishida K, Terashima T, Wolf T, Hardy F, Meingast C, Von Lohneysen H, Levchenko A, Shibauchi T, and Matsuda Y 2016 *Nat. Commun.* **7** 12843
[9] Hanaguri T, Kasahara S, Boker J, Eremin I, Shibauchi T, and Matsuda Y 2019 *Phys. Rev. Lett.* **122** 077001
[10] Takahashi H, Nabeshima F, Ogawa R, Ohmichi E, Ohta H, and Maeda A 2019 *Phys. Rev. B* **99** 060503
[11] Xu B, Munzar D, Dubroka A, Sheveleva E, Lyzwa F, Marsik P, Wang C N, Wang Z C, Cao G H, and Bernhard C 2020 *Phys. Rev. B* **101** 214512
[12] Hao J H, Hong W S, Zhou X X, Xiang Y, Dai Y M, Yang H, Li S L, Luo H Q, and Wen H H 2021 arXiv:2111.04422 [cond-mat.supr-con]
[13] Zhang C, Wu Q Y, Hong W S, Liu H, Zhu S X, Song J J, Zhao Y Z, Wu Y Z, Liu Z T, Liu S Y, Yuan Y H, Huang H, He J, Li S L, Liu H Y, Duan Y X, Luo H Q, and Meng J Q 2021 arXiv:2109.06460 [cond-mat.supr-con]
[14] Wang Q Y, Li Z, Zhang W H, Zhang Z C, Zhang J S, Li W, Ding H, Ou Y B, Deng P, Chang K, Wen J, Song C L, He K, Jia J F, Ji S H, Wang Y Y, Wang L L, Chen X, Ma X C, and Xue Q K 2012 *Chin. Phys. Lett.* **29** 037402
[15] He S L *et al.* 2013 *Nat. Mater.* **12** 605
[16] Tan S Y, Zhang Y, Xia M, Ye Z R, Chen F, Xie X, Peng R, Xu D F, Fan Q, Xu H C, Jiang J, Zhang T, Lai X C, Xiang T, Hu J P, Xie B P, and Feng D L 2013 *Nat. Mater.* **12** 634
[17] Zhang W H *et al.* 2014 *Chin. Phys. Lett.* **31** 017401
[18] Zhang W H, Li Z, Li F S, Zhang H M, Peng J P, Tang C J, Wang Q Y, He K, Chen X, Wang L L, Ma X C, and Xue Q K 2014 *Phys. Rev. B* **89** 060506
[19] Kang B L, Shi M Z, Li S J, Wang H H, Zhang Q, Zhao D, Li J, Song D W, Zheng L X, Nie L P, Wu T, and Chen X H 2020 *Phys. Rev. Lett.* **125** 097003
[20] Ono S and Ando Y 2003 *Phys. Rev. B* **67** 104512
[21] Chen X H, Yu M, Ruan K Q, Li S Y, Gui Z, Zhang G C, and Cao L Z 1998 *Phys. Rev. B* **58** 14219
[22] Xu Y, Rong H T, Wang Q Y, Wu D S, Hu Y, Cai Y Q, Gao Q, Yan H T, Li C, Yin C H, Chen H, Huang J W, Zhu Z H, Huang Y, Liu G D, Xu Z Y, Zhao L, and Zhou X J 2021 *Nat. Commun.* **12** 2840
[23] Faeth B D *et al.* 2021 *Phys. Rev. X* **11** 021054
[24] Wang Z C, He C Y, Tang Z T, Wu S Q, and Cao G H 2017 *Sci. Chin. Mater.* **60** 83
[25] Lu X F, Wang N Z, Wu H, Wu Y P, Zhao D, Zeng X Z, Luo X G, Wu T, Bao W, Zhang G H, Huang F Q, Huang Q Z, and Chen X H 2015 *Nat. Mater.* **14** 325
[26] Miyata Y, Nakayama K, Sugawara K, Sato T, and Takahashi T 2015 *Nat. Mater.* **14** 775
[27] Lei B, Cui J H, Xiang Z J, Shang C, Wang N Z, Ye G J, Luo X G, Wu T, Sun Z, and Chen X H 2016 *Phys. Rev. Lett.* **116** 077002
[28] Berthier C, Julien M H, Horvatic M, and Berthier Y 1996 *J. Phys. I (France)* **6** 2205
[29] Korringa J 1950 *Phys. (Amsterdam)* **16** 601
[30] Alloul H, Ohno T, and Mendels P 1989 *Phys. Rev. Lett.* **63** 1700
[31] Ishida K, Yoshida K, Mito T, Tokunaga Y, Kitaoka Y, Asayama K, Nakayama Y, Shimoyama J, and Kishio K 1998 *Phys. Rev. B* **58** R5960(R)
[32] Dong X L, Jin K, Yuan D N, Zhou H X, Yuan J, Huang Y L, Hua W, Sun J L, Zheng P, Hu W, Mao Y Y, Ma M W, Zhang G M, Zhou F, and Zhao Z X 2015 *Phys. Rev. B* **92** 064515
[33] Wu D P, Meng X D, Zhai Y Y, Yu H M, Yu J, and Qi Y 2019 *Materials* **12** 474
[34] Wang H D, Dong C H, Li Z J, Mao Q H, Zhu S S, Feng C M, Yuan H Q, and Fang M H 2011 *Europhys. Lett.* **93** 47004
[35] Sun S S, Wang S H, Yu R, and Lei H C 2017 *Phys. Rev. B* **96** 064512
[36] Chen G F, Li Z, Dong J, Li G, Hu W Z, Zhang X D, Song X H, Zheng P, Wang N L, and Luo J L 2008 *Phys. Rev. B* **78** 224512
[37] Meier W R, Kong T, Kaluarachchi U S, Taufour V, Jo N H, Drachuck G, Bohmer A E, Saunders S M, Sapkota A, Kreyssig A, Tanatar M A, Prozorov R, Goldman A I, Balakirev F F, Gurevich A, Bud'ko S L, and Canfield P C 2016 *Phys. Rev. B* **94** 064501
[38] Smylie M P, Willa K, Bao J K, Ryan K, Islam Z, Claus H, Simsek Y, Diao Z, Rydh A, Koshelev A E, Kwok W K, Chung D Y, Kanatzidis M G, and Welp U 2018 *Phys. Rev. B* **98** 104503
[39] Vedeneev S I, Piot B A, Maude D K, and Sadakov A V 2013 *Phys. Rev. B* **87** 134512
[40] Wang Z C, Liu Y, Wu S Q, Shao Y T, Ren Z, and Cao G H 2019 *Phys. Rev. B* **99** 144501
[41] Nakamura Y and Uchida S 1993 *Phys. Rev. B* **47** 8369
[42] Kimura T, Kishio K, Kobayashi T, Nakayama Y, Motohira N, Kitazawa K, and Yamafuji K 1992 *Physica C* **192** 247

[43] Ando Y, Boebinger G S, Passner A, Kimura T, and Kishio K 1995 *Phys. Rev. Lett.* **75** 4662
[44] Boebinger G S, Ando Y, Passner A, Kimura T, Okuya M 1, Shimoyama J, Kishio K, Tamasaku K, Ichikawa N, and Uchida S 1996 *Phys. Rev. Lett.* **77** 5417
[45] Terasaki I, Sato Y, Miyamoto S, Tajima S, and Tanaka S 1995 *Phys. Rev. B* **52** 16246
[46] Takenaka K, Mizuhashi K, Takagi H, and Uchida S 1994 *Phys. Rev. B* **50** 6534
[47] Tozer S W, Kleinsasser A W, Penney T, Kaiser D, and Holtzberg F 1987 *Phys. Rev. Lett.* **59** 1768
[48] Hagen S J, Jing T W, Wang Z Z, Horvath J, and Ong N P 1988 *Phys. Rev. B* **37** 7928
[49] Brawner D A, Wang Z Z, and Ong N P 1989 *Phys. Rev. B* **40** 9329
[50] Martin S, Fiory A T, Fleming R M, Schneemeyer L F, and Waszczak J V 1990 *Phys. Rev. B* **41** 846
[51] Wang N L, Buschinger B, Geibel C, and Steglch F 1996 *Phys. Rev. B* **54** 7449
[52] Ando Y, Boebinger G S, Passner A, Wang N L, Geibel C, and Steglich F 1996 *Phys. Rev. Lett.* **77** 2065
[53] Watanabe T, Fujii T, and Matsuda A 1997 *Phys. Rev. Lett.* **79** 2113
[54] Martin S, Fiory A T, Fleming R M, Schneemeyer L F, and Waszczak J V 1988 *Phys. Rev. Lett.* **60** 2194
[55] Fujii T, Watanabe T, and Matsuda A 2001 *J. Cryst. Growth* **223** 175
[56] Fujii T, Terasaki I, Watanabe T, and Matsuda A 2002 *Phys. Rev. B* **66** 024507
[57] Kasahara S, Watashige T, Hanaguri T, Kohsaka Y, Yamashita T, Shimoyama Y, Mizukami Y, Endo R, Ikeda H, Aoyama K, Terashima T, Uji S, Wolk T, H, von L, Shibauchi T, and Matsuda Y 2014 *Proc. Natl. Acad. Sci. USA* **111** 16309
[58] Lubashevsky Y, Lahoud E, Chashka K, Podolsky D, and Kanigel A 2012 *Nat. Phys.* **8** 309
[59] Rinott S, Chashka K, Ribak A, Rienks E D, Taleb-Ibrahimi A, Fevre P L, Bertran F, Randeria M, and Kanigel A 2017 *Sci. Adv.* **3** e1602372
[60] Mizukami Y, Haze M, Tanaka O, Matsuura K, Sano D, Böker J, Eremin I, Kasahara S, Matsuda Y, and Shibauchi T 2021 arXiv:2105.00739v1 [cond-mat.supr-con]
[61] Zhang S Y, Miao G Y, Guan J Q, Xu X F, Liu B, Yang F, Wang W H, Zhu X T, and Guo J D 2019 *Chin. Phys. Lett.* **36** 107404

Supplemental Material:

NMR Evidence for Universal Pseudogap Behavior in Quasi-Two-Dimensional FeSe-Based Superconductors

B. L. Kang(康宝蕾)[1,†], M. Z. Shi(石孟竹)[1,†], D. Zhao(赵丹)[1], S. J. Li(李顺姣)[1], J. Li(李建)[1], L. X. Zheng(郑立玄)[1], D. W. Song(宋殿武)[1], L. P. Nie(聂林鹏)[1], T. Wu(吴涛)[1,2,3,4,5*], and X. H. Chen(陈仙辉)[1,2,3,4,5*]

[1]*Hefei National Research Center for Physical Sciences at the Microscale, University of Science and Technology of China, Hefei, Anhui 230026, China*

[2]*Key Laboratory of Strongly coupled Quantum Matter Physics, Department of Physics, University of Science and Technology of China, Hefei, Anhui 230026, China*

[3]*CAS Center for Excellence in Superconducting Electronics (CENSE), Shanghai 200050, China*

[4]*Collaborative Innovation Center of Advanced Microstructures, Nanjing University, Nanjing 210093, China*

[5]*Hefei National Laboratory, University of Science and Technology of China, Hefei 230088, China*

*Corresponding author. Email: wutao@ustc.edu.cn; chenxh@ustc.edu.cn

†These authors contributed equally to this work

1. Experimental Methods

Crystal growth of $(PY)_xFeSe$. $(PY)_xFeSe$ is synthesized through an electrochemical intercalation process using an FeSe single crystal as the starting material. The process is analogous to that of $(CTA)_xFeSe$ [1] and $(TBA)_xFeSe$ [2]. First, high-quality single crystals of tetragonal FeSe were grown using a KCl-$AlCl_3$ flux method [3]. Second, the weighted FeSe single crystal (~1 mg) is fixed onto an indium wire as the positive electrode, while a silver piece is used as the negative electrode. The electrolyte was obtained by dissolving 0.5 g PY (1-butyl-1-methylpyrrolidinium bromide, TCI, 97%) into 10 ml DMF (N,N-dimethylformamide, Innochem, 99.9%, extra dry with molecular sieves, water less than 50 ppm). The electrochemical intercalation process was controlled by a Lanhe testing system, and here, a constant current of 10 μA was applied. During the current passing through the electrolytic cell, the negative electrode loses electrons, while the

positive electrode obtains electrons. The doping amount x in $(PY)_xFeSe$ is controlled by adjusting the charge passing through the electrolytic cell based on the Faraday law. For a fixed doping amount x, the time t needed can be calculated using the formula $t = Fmx/MI$, where t is the time of the galvanostatic discharge process, F is the Faraday constant (96485.31 C mol^{-1}), m is the mass (g) of the pristine FeSe single crystal, x is the amount of intercalated PY ions, M is the molar mass of FeSe (134.805 g mol^{-1}), and I is the electrical current (A) passing through the cell. In this case, x is set as 1 to achieve uniform and single-phase intercalation. All processes were handled in an argon-filled glove box. The resulting $(PY)_xFeSe$ single crystal maintains a plate-like morphology yet is much thicker.

XRD phase identification and composition analysis. The X-ray diffraction pattern of the sample was collected on a Rigaku SmartLab-9 powder diffractometer with Cu Kα radiation. The composition and actual doping level x in $(PY)_xFeSe$ were determined using an electron probe X-ray microanalyzer (EPMA-8050G, Shimadzu). High-sensitivity qualitative and quantitative elemental analyses, together with element mapping, were applied.

Magnetic and electrical transport measurements. Magnetic susceptibility was measured employing the commercial SQUID-VSM (7 T, Quantum Design). The magnetization was measured in FC and ZFC modes under a magnetic field of 5 Oe. The electrical transport measurements were performed with a Physical Property Measurement System (PPMS-9 T, Quantum Design) by a standard *dc* four-probe method. Considering the air sensitivity of $(PY)_xFeSe$, all the preparation processes for characterization and measurement were handled in an argon-filled glove box, and the samples were coated with a thin layer of chemically stable high-vacuum silicone grease before being taken outside the glove box.

Nuclear magnetic resonance measurements. The standard NMR spin–echo technique was applied using a commercial NMR spectrometer from Thamway Co. Ltd. The external magnetic field was generated by a 12 T magnet from Oxford Instruments. The ^{63}Cu NMR signal from the copper coil was used to calibrate the external field. ^{77}Se NMR spectra were obtained by the fast Fourier transform (FFT) method. The nuclei of ^{77}Se have a nuclear spin $I = 1/2$, and the Knight shift was extracted from the NMR central transition line using the gyromagnetic ratio $\gamma/2\pi = 8.118$ MHz/T. The ^{77}Se spin-lattice relaxation time (T_1) measurements were carried out by using the saturation-recovery method at the peak positions of NMR spectra at all temperatures, and the

spin–echo decay was fitted by a simple exponential function $m(t) = A_0+Aexp[-(t/T_1)^r]$. Error bars are determined by least square fitting to the experimental data.

2. Supplemental Figures and captions

The XRD patterns for pristine FeSe and intercalated $(PY)_xFeSe$ single crystals are shown in Fig. S1.

Figure S2 shows the high-sensitivity EPMA measurement for $(PY)_xFeSe$.

Figure S3 shows the superconducting property for $(PY)_xFeSe$.

Figure S4 offers supplementary information about the NMR measurement for $(PY)_xFeSe$, including the tuning frequency of the NMR coil, the spectra of ^{77}Se nuclei and the temperature evolution of the stretching exponent *r*.

Figure S5 plots the temperature dependence of the Knight shift and $1/T_1T$ for $(PY)_xFeSe$, with an external magnetic field of 12 T being applied in plane and out of plane.

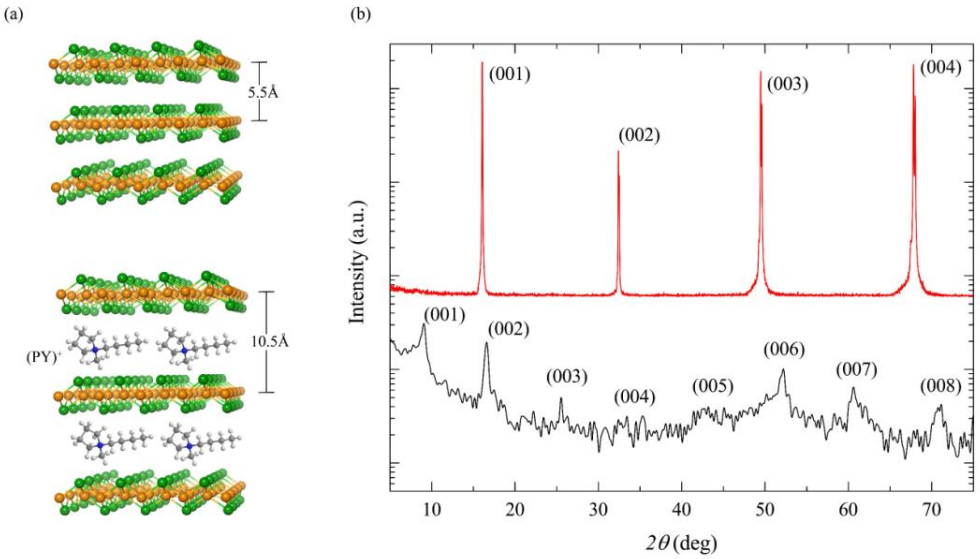

FIG. S1. (a) Crystal structures of pristine FeSe and $(PY)_xFeSe$. The distance between adjacent FeSe layers greatly increased from 5.5 Å to 10.5 Å through the intercalation of PY^+. (b) XRD patterns for FeSe and $(PY)_xFeSe$ single crystals. The (00 l) reflections are well indexed.

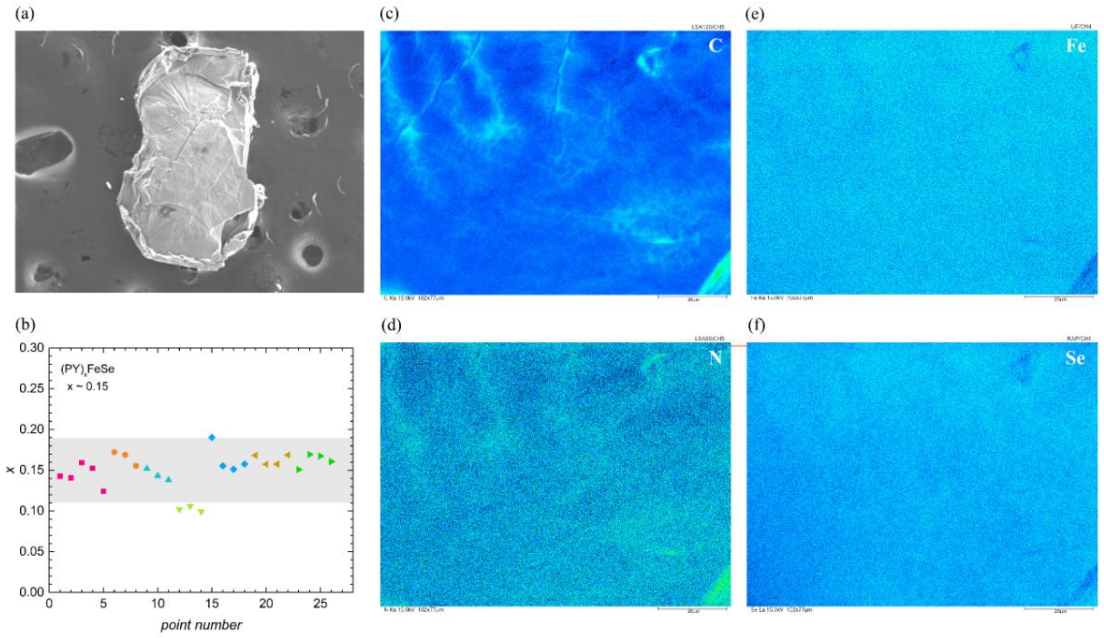

FIG. S2. (a) High-resolution SEM image of a freshly cleaved surface of $(PY)_xFeSe$. (b) Quantitative analysis of the doping level x for $(PY)_xFeSe$. The points labeled in the same color are from different locations of one sample. (c-f) High-definition element mapping analysis in a 102×77 μm area for the main composition elements, including C, N, Fe and Se.

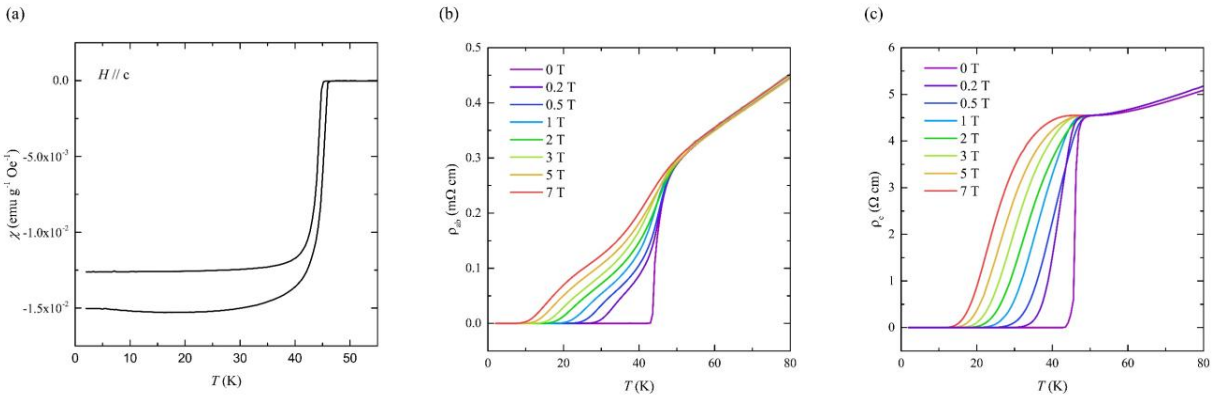

FIG. S3. (a) Temperature dependence of magnetic susceptibility measured in FC and ZFC modes under a magnetic field of 5 Oe. (b) The temperature dependence of the in-plane resistivity under different magnetic fields applied along the c axis. The fan-shaped broadening under magnetic fields indicates a strong 2D characteristic. (c) Temperature dependence of the out-of-plane resistivity under different magnetic fields applied along the c axis.

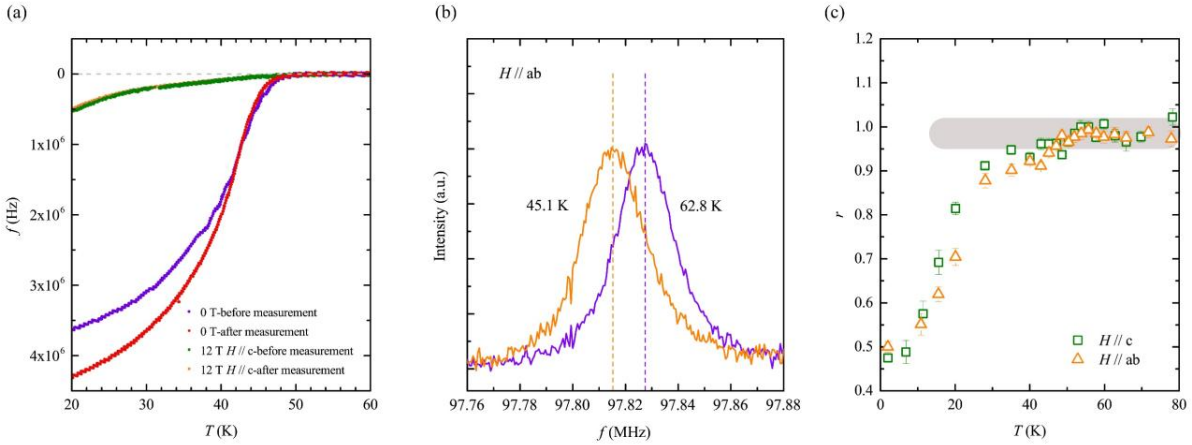

FIG. S4. (a) Tuning frequency of the NMR coil before and after the NMR measurements. The frequency shift indicates a clear superconducting transition. (b) NMR spectra of ^{77}Se nuclei measured at 45.1 K and 62.8 K, respectively. The uniform frequency shift of the NMR spectrum without obvious distortion or broadening indicates an intrinsic change in the Knight shift below T_p. (c) Temperature evolution of the stretching exponent r. The value of r is extracted from the T_1 fitting by the stretched exponential function. It remains nearly constant in the temperature range between T_{c0} and T_p.

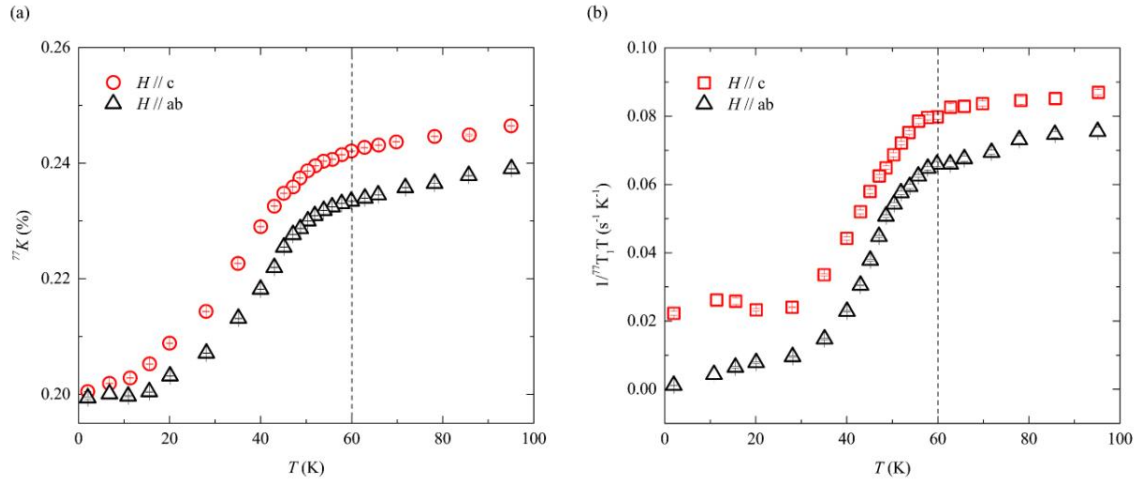

FIG. S5. (a) Temperature dependence of the Knight shift for $(PY)_xFeSe$. (b) Temperature dependence of the spin-lattice relaxation rate divided by temperature $1/T_1T$ for $(PY)_xFeSe$. The external magnetic field is 12 T in (a) and (b). The vertical dashed lines at ~ 60 K indicate the onset temperature of local superconducting pairing.

.

Reference:

[1] M. Z. Shi, N. Z. Wang, B. Lei, C. Shang, F. B. Meng, L. K. Ma, F. X. Zhang, D. Z. Kuang, and X. H. Chen, Phys. Rev. Mater. 2, 074801 (2018).

[2] M. Z. Shi, N. Z. Wang, B. Lei, J. J. Ying, C. S. Zhu, Z. L. Sun, J. H. Cui, F. B. Meng, C. Shang, L. K. Ma, and X. H. Chen, New J. Phys. 20, 123007 (2018).

[3] D. Chareev, E. Osadchii, T. Kuzmicheva, J. Y. Lin, S. Kuzmichev, O. Volkova, and A. Vasiliev, CrystEngComm 15, 1989 (2013).